

## Broadband antireflection on the silicon surface realized by Ag nanoparticle-patterned black silicon

Cite this: *Phys. Chem. Chem. Phys.*, 2013, **15**, 2345

Y. Wang,<sup>ab</sup> Y. P. Liu,<sup>\*ab</sup> H. L. Liang,<sup>ab</sup> Z. X. Mei<sup>\*ab</sup> and X. L. Du<sup>ab</sup>

Broadband antireflection of silicon has been realized by combining black silicon, surface passivation and surface plasmons. Black silicon, fabricated by Ag assisted chemical etching, was employed here to reduce the reflection of incident light with wavelengths below 1100 nm. Due to the increased bandgap caused by the quantum confinement effect and enhanced backward-scattering in our black silicon, light trapping was diminished at the wavelengths above 1100 nm. Ag nanoparticles were deposited on black silicon to obtain the lowest reflectivity at the wavelengths above 1100 nm. Compared with traditionally textured multicrystalline silicon, the average reflectivity of passivated black multicrystalline silicon patterned with 5 nm mass thickness of Ag was decreased to 5.7% in the wavelength range from 300 nm to 1100 nm and was reduced by 20.2% in the wavelength range from 1100 nm to 1400 nm. The surface plasmon effect of the Ag nanoparticles on the black silicon was also demonstrated by surface enhanced Raman scattering, which was observed in the Ag nanoparticle patterned black silicon after being immersed in rhodamine 6g.

Received 25th September 2012,  
Accepted 7th December 2012

DOI: 10.1039/c2cp44406b

[www.rsc.org/pccp](http://www.rsc.org/pccp)

### Introduction

Reflectivity of flat silicon, an indirect band gap semiconductor, is more than 30%, which shows a very low absorption coefficient. In order to reduce such light loss, pyramidal structures are commonly fabricated on the crystalline silicon (c-Si) surface by anisotropic etching with alkali, while 'worm like' structures are applied to the multicrystalline silicon (mc-Si) surface by isotropic etching with acid. However, even after texturing, the reflectivity is about 10% for c-Si and 20% for mc-Si in the wavelength range from 300 to 1000 nm, respectively.

Black silicon has drawn a lot of attention in recent years because of its extensive application in photodetectors, luminescent devices, sensors and silicon based solar cells.<sup>1–3</sup> For solar cell applications, black silicon has a great advantage in light trapping. It was first discovered in the 1980s as an unwanted side effect of reactive ion etching (RIE), but in 1998 it was purposefully developed in Eric Mazur's laboratory by using femtosecond laser pulses.<sup>4</sup> R. Dussart *et al.* also employed plasma technology to fabricate black silicon.<sup>5</sup> However, it is

both expensive and inefficient to use laser or plasma technology for large-area black silicon texturing. After that, an electrochemical etching technique was developed by C. C. Striemer and Fauchet<sup>6</sup> and L. L. Ma *et al.*<sup>7</sup> to obtain low reflectivity over a broad spectral range by continuously controlling over the porosity of a porous silicon layer. However, electrochemical etching needs external current and electrodes, which is not very convenient for mass production. After that, metal-assisted chemical etching has been widely researched for black silicon solar cells because of its low cost and simple process. Noble metal nanoparticles (NPs) such as Pt, Au, Ag and Cu were usually deposited as a catalyst first, and then an aqueous solution of HF and H<sub>2</sub>O<sub>2</sub> was used to etch silicon. Recently, NREL<sup>3,8</sup> reported one-step fabrication of an Au NP-assisted black silicon solar cell with 16.8% efficiency. Au NPs were obtained by immersing the polished p-type silicon (100) substrate in 0.4 mM HAuCl<sub>4</sub> solution added with an equal quantity of HF–H<sub>2</sub>O<sub>2</sub>–H<sub>2</sub>O (1 : 5 : 2) mixture for several minutes. After metal assisted etching, the reflectivity of the silicon substrate was reduced to 2% from 300 nm to 1000 nm without any antireflective (AR) coating. As reported previously, we have used AgNO<sub>3</sub>–HF solution to fabricate large-area black silicon on both c-Si and mc-Si by a one-step method. The average reflectivity was reduced as low as 2% for c-Si and 4% for mc-silicon, from 300 to 1000 nm with no AR coating.<sup>9</sup> However, as we found in the experiment, although this black silicon had an amazing antireflection function below 1000 nm wavelength,

<sup>a</sup> Beijing National Laboratory for Condensed Matter Physics, Institute of Physics, Chinese Academy of Sciences, Beijing 100190, China.  
E-mail: zxmei@aphy.iphy.ac.cn, ypliu@aphy.iphy.ac.cn

<sup>b</sup> Key Laboratory for Renewable Energy, Chinese Academy of Sciences, Beijing Key Laboratory for New Energy Materials and Devices, Beijing 100190, China

the reflectivity above 1100 nm was higher than alkali or acid textured samples. Therefore, the new challenge was to figure out a special technique for black silicon to achieve broadband antireflection with lower reflectivity above 1100 nm.

Surface plasmons (SPs) effect is another effective method to reduce the reflectivity of silicon. It opens a new way to tailor and amplify the incident light, which can be widely applied to biomedical, energy,<sup>10–12</sup> environment protection, sensing, and information technology. Surface plasmons are collective oscillations of conduction electrons that exist in metal particles. When the frequency of incident light photons matches the natural frequency of conduction electrons oscillating against the restoring force of polarization charges, the metal particles strongly interact with incident light, named surface plasmon resonance (SPR). The resonant frequency of surface plasmons depends on the particle geometry, material and the local environment.<sup>10,11</sup> Near the surface plasmon resonance frequency, the interactional cross-sectional area between incident light and metal particle is much larger than the geometric cross section of the metal particle.<sup>10</sup> The interactional cross section of the noble metal NPs can be up to 10 times their geometrical section. On the other hand, SPR is considered to be one of the reasons for surface enhanced Raman scattering (SERS).<sup>13</sup> When some molecules are adsorbed on certain rough metal (Au, Ag, Cu) surfaces, the Raman scattering intensity of these molecules will be much larger than that under normal circumstances – this phenomenon is called SERS. Accordingly, SERS is a useful technique to demonstrate the existence of the SPR effect on the metal NPs.

For solar cell applications, SPs can effectively enhance the light trapping ability of the cell. Ag NPs are a promising candidate for the light trapping of silicon solar cells due to their low absorption and powerful ability of coupling the incident light into the cells over a large angular range. S. Pillai *et al.*<sup>10</sup> found that the photocurrent where the wavelength of the incident light was above 1100 nm could be significantly improved by depositing thin Ag film onto the surface of a silicon solar cell. Very recently, Zhida Xu *et al.*<sup>13</sup> produced a black silver c-Si wafer by depositing 5 nm titanium and 80 nm silver onto nanocone forest structures fabricated by RIE. The average reflectivity in the wavelength range from 200 to 1100 nm was 9.9%. However, the RIE technique is expensive and a continuous, thick Ag film structure is not considered suitable for solar cell fabrication.

In this letter, we adopt one-step Ag assisted chemical etching to fabricate black silicon on a conventionally acid treated mc-Si wafer. The reflectivity drops significantly to less than 10% over the spectral range from 200 to 1000 nm. In order to reduce the loss of long wavelength light above 1100 nm, Ag NPs were deposited onto the black silicon. For further application in silicon solar cells, a SiN<sub>x</sub> dielectric layer was deposited by PECVD before the deposition of the Ag NPs. The SiN<sub>x</sub> layer was introduced for two purposes: passivating the black silicon and isolating the Ag NPs from it. Finally, the reflection of incident light above 1100 nm was effectively suppressed on the black silicon.

## Experimental details

Commercially used 156 mm × 156 mm p-type mc-Si with a resistivity of 1–3 Ω cm and a thickness of 200 ± 20 μm had been cut into 50 mm × 50 mm pieces for experimental use. The pieces were first soaked in alcohol, acetone and deionized water in a sonication bath for 5 minutes, respectively, and then immersed in HNO<sub>3</sub>–HF–CH<sub>3</sub>COOH mixed solution for 70 seconds to remove the saw damage on the silicon surface. The black silicon was fabricated by Ag catalyzed chemical etching in a polytetrafluoroethylene container with 4.0 M HF and 0.01 M AgNO<sub>3</sub> mixture at room temperature for 2 minutes. Then the silver contamination on the silicon surface was removed by HNO<sub>3</sub> in a sonication bath for 5 minutes, followed by rinsing with deionized water and dried by blowing nitrogen. A 30 nm SiN<sub>x</sub> layer was deposited onto the black silicon surface by PECVD before Ag NPs deposition. We prepared different mass thicknesses of Ag by the thermal evaporation technique. For comparison, the same mass thickness of Ag was deposited both on acid textured silicon wafer and black silicon. A Varian Cary 5000 spectrophotometer with an integrating sphere was used to measure total hemispherical reflectance for normal incidence. A Hitachi S-4800 scanning electron microscope (SEM) was used for characterizing the morphology and structures of the samples. An InVia-Reflex Micro-Raman Spectroscopy System with a 532 nm excitation source was employed to measure SERS of rhodamine 6g (R6g).

## Results and discussion

Fig. 1(a) shows the SEM image of the conventionally acid textured silicon surface. Fig. 1(b) is the SEM surface morphology of the black silicon etched in AgNO<sub>3</sub>–HF solution for 2 minutes. Pillar-like nanostructures can be observed on the etched silicon surface, where the height of a nanopillar is about 90 nm.

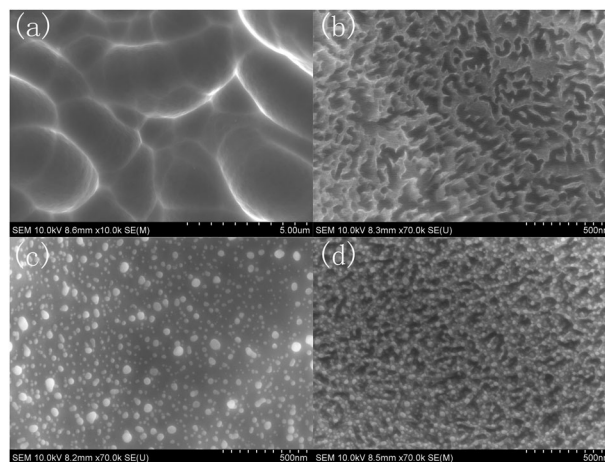
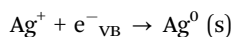


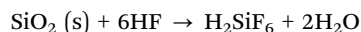
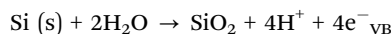
**Fig. 1** (a) SEM image of the conventionally acid textured Si surface. (b) SEM image of black silicon which was etched in AgNO<sub>3</sub>–HF solution for 3 minutes with removal of Ag. (c) SEM image of acid textured Si deposited with 5 nm mass thickness of Ag. (d) SEM image of black Si deposited with 5 nm mass thickness of Ag.

For the typical metal-assisted chemical etching procedure, a silicon substrate is partly covered by noble metal which can be obtained by vacuum technology or electroless deposition. Due to the catalysis, the silicon beneath the noble metal is etched much faster than that exposed to the solution. As the etching proceeds, the noble metal sinks below the surface, resulting in pores or wires whose forms depend on the initial morphology of the noble metal coverage.<sup>14</sup> In this work, Ag was electrolessly deposited onto the substrate's surface by immersing silicon in  $\text{AgNO}_3\text{-HF}$  solution at the beginning. The driving force of this electrochemical reaction is the electrochemical potential difference between silicon and  $\text{Ag}^+/\text{Ag}$ .<sup>14</sup> The reaction can be described as two half-cell reactions.<sup>15</sup>

Cathode reaction:



Anode reaction:



In this case, the  $\text{Si-AgNO}_3\text{-HF}$  system is composed of a corrosion-type redox couple: the cathodic reduction of  $\text{Ag}^+$  ions, and the anodic oxidation and dissolution of silicon beneath the deposited Ag. After adhering to the silicon surface, the Ag nuclei easily attracts electrons from the silicon substrate, which catalyzes the reduction of  $\text{Ag}^+$  in the solution, resulting in the growth of Ag nuclei. Simultaneously, the silicon beneath Ag particles is oxidized to  $\text{SiO}_2$  and then dissolved by HF, so that Ag particles sink and leave holes in the upper silicon surface. As the reaction proceeds, the density of Ag particles adhering to the silicon surface reaches saturation, and then Ag particles begin to grow into branched silver dendrites.<sup>15,16</sup> Finally, as the silicon beneath Ag particles is etched away to a certain depth, silicon nanopillar structures appear.

As shown in Fig. 2, the average reflectivity of the resulting black silicon in the wavelength range from 300 nm to 1100 nm is 8.2%, while that of conventionally acid textured silicon is 28.6%.

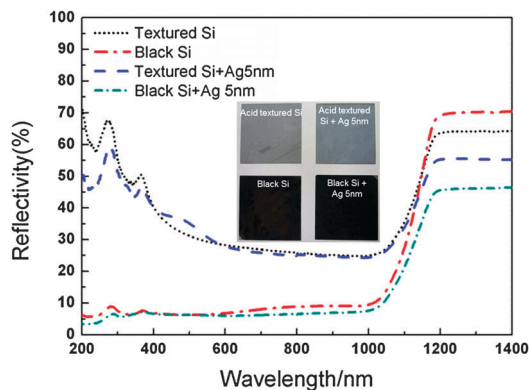


**Fig. 2** Total hemispherical reflectance of acid textured Si, black Si, acid textured Si with 5 nm mass thickness of Ag, and black Si with 5 nm mass thickness of Ag. Inset is a photograph of these four samples.

The light trapping ability is significantly enhanced by the nanopillar structures, which is illustrated by the change of the sample's appearance (inset of Fig. 2). The appearance of the acid textured silicon obviously turns to dim gray after the nanopillar structures form. Generally, light trapping of conventionally textured silicon is mostly governed by multiple reflections,<sup>17</sup> while the superior antireflection property of black silicon can be attributed to two reasons. First, the porosity of the nanopillars decreases from their top to their bottom, gradually modulating the effective refractive index – in effect, resembling a multilayer antireflective coating.<sup>7,18</sup> The extent of reflection mainly depends on the difference of the refractive index between two media, the more similar refractive index, the less reflection will be. Thus, broadband suppression in reflectance can be achieved by inserting a dielectric layer which gradually changed the refractive index between air and silicon. In this letter, nanopillars with varied porosities act as such a dielectric layer. Second, as can be observed from the SEM image, the surface of the nanopillars is rather rough, which scatters and absorbs more light than a flat surface.<sup>18</sup>

However, the reflectivity of our black silicon increased more rapidly than conventionally acid textured silicon above 1100 nm (Fig. 2). In our understanding, this phenomenon should be mainly attributed to the increased band gap caused by the quantum confinement effect and the enhanced backward-scattering caused by nanopillars. As can be seen in Fig. 1(b), the diameters of the nanopillars vary from several nanometers to several tens of nanometers. The diameters of small nanopillars are even less than 5 nm, just equal to or smaller than the 4.9 nm Bohr exciton radius of bulk silicon.<sup>19</sup> When the size of the nanostructure decreases to approach the radius of the Bohr exciton, the movement of charge carriers will be limited, resulting in an increase of kinetic energy and a change of the original continuous band to quasi-discrete energy levels, which increases the effective band gap. This phenomenon of silicon nanostructures, such as silicon nanowires,<sup>19</sup> porous silicon<sup>20</sup> and silicon nanocrystals,<sup>21</sup> has already been reported before. In the case of our black etched silicon, the quantum confinement effect also could be expected to exist. On the other hand, the interaction between incident infrared light and nanostructures was enhanced because of the larger surface area introduced by silicon nanostructures. However, the black silicon nanostructures had a wider band gap than the acid textured Si wafer, so the black silicon could not absorb the infrared light which interacted with it but just enhanced the backward scattering.<sup>3</sup> Herein, we think it is reasonable that the reflection of the black silicon is a bit more than that of acid textured silicon above 1100 nm.

Fig. 1(c) is the SEM image of acid textured silicon deposited with 5 nm mass thickness of Ag by thermal evaporation, the diameters of Ag NPs range from about 15 nm to 50 nm. Fig. 1(d) also shows the SEM image of black silicon patterned with 5 nm mass thickness of Ag prepared by thermal evaporation. However, the average diameter of Ag NPs on the black silicon surface was 18 nm, obviously smaller and denser than the ones



on acid textured silicon. This could be explained by the difference of substrates' surface structures. The surface of the acid textured sample is relatively smooth, so it is easy for Ag atoms and Ag clusters to migrate and merge after being deposited on the substrate, leading to bigger Ag NPs. In contrast, the black silicon surface was rather rough, so it was relatively hard for the Ag atoms and Ag clusters to cross the potential energy barrier to combine with each other. In this case, it was difficult for Ag NPs to move and merge into bigger ones after being deposited on the black silicon surface.

As shown in Fig. 2, the reflectivity of the Ag NP-patterned, conventionally textured mc-Si is 7.5% lower in the wavelength range from 1100 nm to 1400 nm. Similarly, the light trapping ability of the Ag NP patterned black silicon is even better, especially around the bandgap of silicon, the average reflectivity is 19.6% lower (from 63.9% to 44.3%) in the wavelength range from 1100 nm to 1400 nm, and is only 6.0% compared to 8.2% in the wavelength range from 300 nm to 1100 nm. The enhancement of light trapping is attributed to SPR caused by collective oscillations of conduction electrons of the Ag NPs. Acting as a scattering medium, the Ag NPs successfully increase the interactional cross-sectional area with incident light, effectively couple the incident light into the silicon substrate over a large angular range, and trap the light inside the active region. As can be observed in Fig. 2, Ag NPs play a key role in enhancing light trapping performance at long wavelengths close to the bandgap, but make little difference in the visible region. In this case, we suggest that the bulk silicon is thick enough to absorb visible and ultraviolet light, so the enhancement in these regions is not so prominent.<sup>10</sup>

For solar cell fabrication, Ag NPs cannot be deposited directly on a naked black silicon surface because of a tendency toward interdiffusion of Ag and silicon atoms. Hence, before the Ag deposition, a 30 nm SiN<sub>x</sub> layer was covered on all samples. First, as a conventional passivation layer for silicon solar cells, SiN<sub>x</sub> was employed here to reduce dangling bonds on the black silicon surface and increase the effective lifetime of minority carriers. Second, the SiN<sub>x</sub> layer was introduced to suppress the coupling and interdiffusion between Ag NPs and black silicon. Fig. 3(a) is the SEM image of black silicon covered with 30 nm SiN<sub>x</sub> (sample A). Fig. 3(b)–(d) show the passivated black silicon patterned with 3 nm, 5 nm and 10 nm mass thicknesses of Ag (sample B, sample C and sample D), respectively. The Ag NPs sizes of sample B are relatively small and uniform with an average of 10 nm diameter. When the mass thickness of evaporated Ag increases to 5 nm (sample C), Ag NPs grow bigger and the average diameter of Ag NPs increases to 18 nm. For sample D, the mass thickness of Ag is twice that of sample C and the Ag NPs are larger – about 25 nm in diameter.

The reflectance spectra of these four samples are shown in Fig. 4(a). Covered with the 30 nm SiN<sub>x</sub> layer, the reflectivity of black Si is slightly lower across the whole spectrum range from 200 nm to 1400 nm. The reflectivity of three samples patterned with Ag NPs is lower in the wavelength range from 1100 nm to 1400 nm by varied degrees. An inconsistent reflection increase is observed in the visible range from 300 nm to 800 nm.

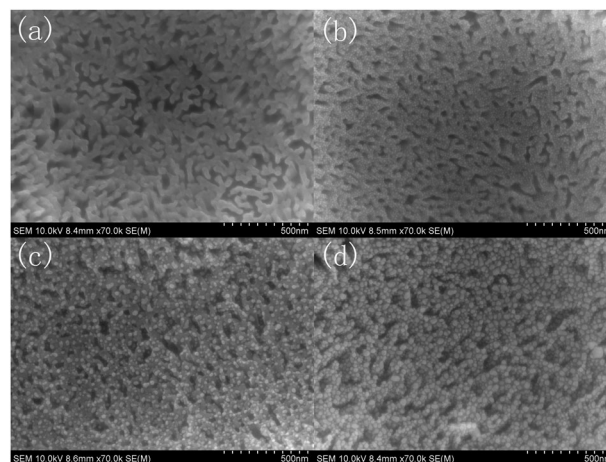


**Fig. 3** SEM image of black Si covered with a 30 nm SiN<sub>x</sub> layer and different mass thicknesses of Ag: (a) 0 nm mass thickness of Ag, (b) 3 nm mass thickness of Ag, (c) 5 nm mass thickness of Ag, and (d) 10 nm mass thickness of Ag.

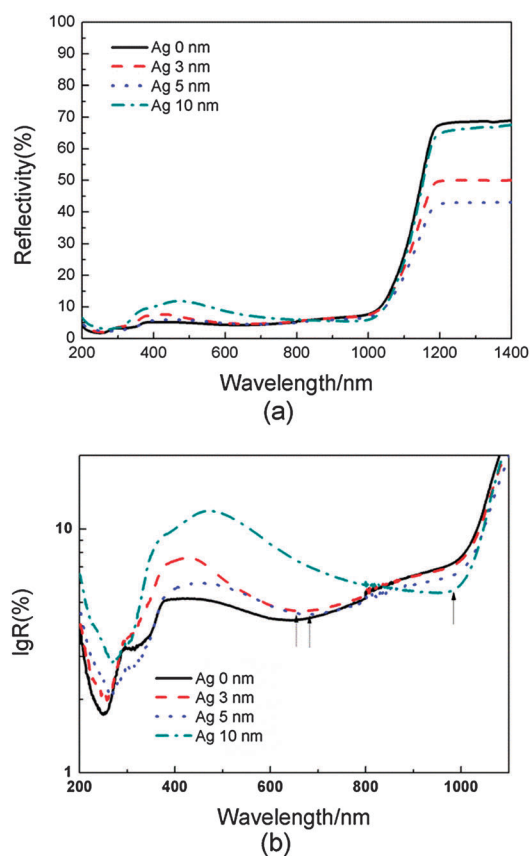


**Fig. 4** (a) Total hemispherical reflectance of black Si covered with a 30 nm SiN<sub>x</sub> layer and 0 nm, 3 nm, 5 nm, 10 nm mass thickness of Ag. (b) Logarithmic transformation of (a).

Doubtlessly, the difference here is attributable to the presence of different sizes of Ag NPs. When the wavelength of incident light is shorter than the surface plasmon polariton resonance wavelength of Ag NPs, the polarizability phase of the Ag NPs is

nonzero, resulting in disadvantageous interference between the transmitted and scattered field components, and finally resulting in the increase in reflectivity. While the wavelength of incident light increases to be longer than the SPR wavelength of Ag NPs, the Ag NPs have zero polarizability phase, leading to advantageous interference between the transmitted and scattered field components and consequently a decrease of reflection,<sup>22,23</sup> so we can observe an increase of reflectivity in the range from 200 nm to 800 nm and a decrease of reflectivity in the range from 1100 nm to 1400 nm.<sup>10</sup> For more detail, Fig. 4(b) is a logarithmic transformation of Fig. 4(a) showing that with the increase in Ag NPs size, the reflectivity peak valleys in the wavelength range from 400 nm to 1100 nm undergo a redshift. The larger the Ag NPs, the greater the redshift and the broader the peak of SPR. For small Ag NPs, the scattering is dominated by dipolar modes. As the size of Ag NPs increases, higher order multipolar modes are excited, diminishing the trapping of light. The average reflectivity of sample C is 5.7% in the wavelength range from 300 nm to 1100 nm and 39.7% in the wavelength range from 1100 nm to 1400 nm. Its total average reflectivity is 9.3% in the wide wavelength range from 300 nm to 1400 nm. These measurements show that sample C is the most suitable of the three samples for broadband antireflection in silicon solar cells because its patterned Ag NPs are of optimal size for the application.

For further study, SERS was carried out to better understand the SP effect of the Ag NP patterned black silicon. At first, seven different kinds of samples were immersed in 1 mM R6g solution for 5 hours, and then dried by nitrogen. A laser with a wavelength of 532 nm was adopted for Raman excitation. Fig. 5 shows the Raman spectra of these samples. No peak was observed in the Raman spectra of acid textured silicon (curve (A)) or black silicon (curve (C)). When these two samples are deposited with 5 nm mass thickness of Ag, nine peaks with wavenumbers of 613  $\text{cm}^{-1}$ , 774  $\text{cm}^{-1}$ , 1127  $\text{cm}^{-1}$ , 1184  $\text{cm}^{-1}$ , 1310  $\text{cm}^{-1}$ , 1363  $\text{cm}^{-1}$ , 1508  $\text{cm}^{-1}$ , 1575  $\text{cm}^{-1}$ , 1650  $\text{cm}^{-1}$  appear in the Raman spectra (curve (B) and curve (D)), which were identified as characteristic peaks of R6g.<sup>24</sup> The four peaks at 613  $\text{cm}^{-1}$ , 774  $\text{cm}^{-1}$ , 1127  $\text{cm}^{-1}$  and 1184  $\text{cm}^{-1}$  are attributed to in-plane or out-of-plane deformation vibrations of the benzene ring, whereas the other five peaks are caused by C=C double bond stretching vibration of the benzene ring.<sup>25,26</sup> The SERS effect of black silicon

patterned with 5 nm mass thickness of Ag is much stronger than that of acid textured silicon covered with the same mass thickness of Ag. This can be explained by: (1) the SERS effect, enhanced by the roughness of the black silicon surface,<sup>27</sup> and (2) the decreased sizes of Ag NPs (as mentioned before). Curves (E)–(G) are Raman spectra of black silicon patterned with 3 nm, 5 nm, 10 nm mass thicknesses of Ag after 30 nm  $\text{SiN}_x$  deposition. Curve (F) shows the most obvious increase in the intensity of R6g characteristic peaks, consistent with the reflectivity results shown in Fig. 4(a). Compared to curve (D), the Raman scattering intensity of curve (F) was significantly greater, where the enhancement of SERS can be attributed to the presence of the  $\text{SiN}_x$  layer. With the  $\text{SiN}_x$  layer, the interference between the incident light and the partially reflected scattered field becomes weaker, contributing to the increase of dipolar mode coupling.<sup>28</sup>

## Conclusions

In conclusion, we have successfully fabricated black silicon on conventionally acid textured mc-Si by one-step Ag assisted chemical etching. However, the quantum confinement effect was observed because of the presence of small nanopillars on the black silicon surface. Both increased band gap and enhanced backward-scattering resulted in the enhancement of the reflectivity near the silicon band gap. Ag NPs were employed to reduce the light trapping loss at long wavelengths. Before Ag NP fabrication, a 30 nm  $\text{SiN}_x$  layer was deposited onto the black silicon surface for black silicon passivation and to isolate the Ag NPs from the black silicon substrate. In order to obtain a suitable size of Ag NPs, different mass thicknesses of Ag (3 nm, 5 nm, 10 nm) were deposited onto the black silicon with the 30 nm  $\text{SiN}_x$  layer. As the size of Ag NPs increases, the surface plasmon resonance peak in the wave range from 400 nm to 1100 nm undergoes a redshift, and the scattering modes change from dipolar modes to higher order multipolar modes. SERS was also observed in an Ag NP patterned black silicon and a rhodamine 6g system, which was used to demonstrate the existence of the SPR effect in the Ag NPs. Finally, broadband antireflection of mc-Si was achieved by combining black silicon, surface passivation and surface plasmons. For further research, solar cells will be fabricated based on the above mentioned structure, and will be studied in our follow-on work.

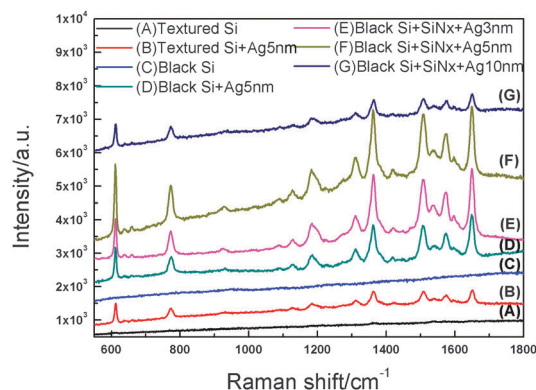


Fig. 5 SERS of rhodamine 6g with different substrates.

## Acknowledgements

This work was supported by the Ministry of Science and Technology (Grant no. 2011CB302002, 2009CB929404) of China, the National Science Foundation (Grant no. 11174348, 61076007, 61204067, 11274366, 51272280).

## References

- 1 S. Koynov, M. S. Brandt and M. Stutzmann, *Appl. Phys. Lett.*, 2006, **88**, 203107.
- 2 J. S. Yoo, I. O. Parm, U. Gangopadhyay, K. Kim, S. K. Dhungel, D. Mangalaraj and J. Yi, *Sol. Energy Mater. Sol. Cells*, 2006, **90**, 3085.

- 3 H. C. Yuan, V. E. Yost, M. R. Page, P. Stradins, D. L. Meier and H. M. Branz, *Appl. Phys. Lett.*, 2009, **95**, 123501.
- 4 T. H. Her, R. J. Finlay, C. Wu, S. Deliwala and E. Mazur, *Appl. Phys. Lett.*, 1998, **73**, 1673.
- 5 R. Dussart, X. Mellhaoui, T. Tillocher, P. Lefauchaux, M. Volatier, C. S. Clerc, P. Brault and P. Ranson, *J. Phys. D: Appl. Phys.*, 2005, **38**, 3395.
- 6 C. C. Striemer and P. M. Fauchet, *Appl. Phys. Lett.*, 2002, **81**, 2980.
- 7 L. L. Ma, Y. C. Zhou, N. Jiang, X. Lu, J. Shao, W. Lu, J. Ge, X. M. Ding and X. Y. Hou, *Appl. Phys. Lett.*, 2006, **88**, 171907.
- 8 H. M. Branz, V. E. Yost, S. Ward, K. M. Jones, B. To and P. Stradins, *Appl. Phys. Lett.*, 2009, **94**, 231121.
- 9 Y. P. Liu, T. Lai, H. L. Li, Y. Wang, Z. X. Mei, H. L. Liang, Z. L. Li, F. M. Zhang, W. J. Wang, A. Y. Kuznetsov and X. L. Du, *Small*, 2012, **9**, 1392.
- 10 S. Pillai, K. R. Catchpole, T. Trupke and M. A. Green, *J. Appl. Phys.*, 2007, **101**, 093105.
- 11 F. J. Beck, S. Mokkaapati and K. R. Catchpole, *Prog. Photovoltaics*, 2010, **18**, 500.
- 12 Y. Yang, S. Pillai, H. Mehravrz, H. Kampwerth, A. H. Baillie and M. A. Green, *Sol. Energy Mater. Sol. Cells*, 2012, **101**, 217.
- 13 Z. D. Xu, Y. Chen, M. R. Gartia, J. Jiang and G. L. Liu, *Appl. Phys. Lett.*, 2011, **98**, 241904.
- 14 Z. P. Huang, N. Geyer, P. Werner, J. D. Boor and U. Gösele, *Adv. Mater.*, 2011, **23**, 285.
- 15 K. Q. Peng, J. J. Hu, Y. J. Yan, Y. Wu, H. Fang, Y. Xu, S. T. Lee and J. Zhu, *Adv. Funct. Mater.*, 2006, **16**, 387.
- 16 K. Q. Peng, Y. J. Yan, S. P. Gao and J. Zhu, *Adv. Funct. Mater.*, 2003, **13**, 127.
- 17 V. V. Iyengar, B. K. Nayak and M. C. Gupta, *Sol. Energy Mater. Sol. Cells*, 2010, **94**, 2251.
- 18 S. K. Srivastava, D. Kumar, P. K. Singh, M. Kar, V. Kumar and M. Husain, *Sol. Energy Mater. Sol. Cells*, 2010, **94**, 1506.
- 19 A. R. Guichard, D. N. Barsic, S. Sharma, T. I. Kamins and M. L. Brongersma, *Nano Lett.*, 2006, **6**, 2140.
- 20 C. Delerue, G. Allan and M. Lannoo, *Phys. Rev. B: Condens. Matter Mater. Phys.*, 1993, **48**, 11024.
- 21 T. Y. Kim, N. M. Park, K. H. Kim, G. Y. Sung, Y. W. Ok, T. Y. Seong and C. J. Choi, *Appl. Phys. Lett.*, 2004, **85**, 5355.
- 22 S. H. Lim, W. Mar, P. Matheu, D. Derkacs and E. T. Yu, *J. Appl. Phys.*, 2007, **101**, 104309.
- 23 F. J. Beck, A. Polman and K. R. Catchpole, *J. Appl. Phys.*, 2009, **105**, 114310.
- 24 P. Hildebrandt and M. Stockburger, *J. Phys. Chem.*, 1984, **88**, 5935.
- 25 I. Talian, K. B. Mogensen, A. Oriňák, D. Kaniansky and J. Hübner, *J. Raman Spectrosc.*, 2009, **40**, 982.
- 26 Z. Yi, X. B. Xu, X. B. Li, J. S. Luo, W. D. Wu, Y. J. Tang and Y. G. Yi, *Appl. Surf. Sci.*, 2011, **258**, 212.
- 27 J. N. Chen, T. Martensson, K. A. Dick, K. Deppert, H. Q. Xu, L. Samuelson and H. X. Xu, *Nanotechnology*, 2008, **19**, 275712.
- 28 K. R. Catchpole and A. Polman, *Appl. Phys. Lett.*, 2008, **93**, 191113.